Nat. Hazards Earth Syst. Sci. Discuss., 2, 7735–7772, 2014
www.nat-hazards-earth-syst-sci-discuss.net/2/7735/2014/
doi:10.5194/nhessd-2-7735-2014

Natural Hazards and Earth System Sciences
Open Access
Discussions

Inversion method for initial tsunami waveform reconstruction

V. V. Voronin[1], T. A. Voronina[2], and V. A. Tcheverda[3]

[1]Novosibirsk State University, Novosibirsk, Russia
[2]Institute of Computational Mathematics and Mathematical Geophysics of SB RAS, Novosibirsk, Russia
[3]A. A. Trofimuk Institute of Petroleum Geology and Geophysics SB RAS, Novosibirsk, Russia

Received: 20 November 2014 – Accepted: 24 November 2014 – Published: 17 December 2014

Correspondence to: T. A. Voronina (tanvor@bk.ru)

Published by Copernicus Publications on behalf of the European Geosciences Union.

Abstract

This paper deals with the application of r-solution method to recover the initial tsunami waveform in a tsunami source area by remote water-level measurements. Wave propagation is considered within the scope of a linear shallow-water theory. An ill-posed inverse problem is regularized by means of least square inversion using a truncated SVD approach. The properties of obtained solution are determined to a large extent by the properties of an inverse operator, which were numerically investigated. The method presented allows one to control instability of the numerical solution and to obtain an acceptable result in spite of ill-posedness of the problem. It is shown that the accuracy of tsunami source reconstruction strongly depends on the signal-to-noise ratio, the azimuthal coverage of recording stations with respect to the source area and bathymetric features along the wave path. The numerical experiments were carried out with synthetic data and various computational domains including a real bathymetry. The method proposed allows us to make a preliminary prediction of the efficiency of the inversion with a given set of the recording stations and to find out the most informative part of the existing observation system. This essential property of the method can prove to be useful in designing a monitoring system for tsunamis.

1 Introduction

Recently, all of us were witnesses of the terrible tsunami that occurred on 11 March 2011 off the coast of Japan. The tsunami in Japan resembled a disaster in the Indian Ocean in 2004. These mega-events prompted serious efforts to address the mitigating threats posed by the tsunamis.

An increasing reliability of the tsunami prediction can partially be achieved with numerical modeling, which allows estimating the expected propagation, as well as run up, wave heights and arrival times of a tsunami in protected regions. An important part of tsunami simulation is to gain some insight into the tsunami source. The modern

NHESSD
2, 7735–7772, 2014

tsunami early warning systems conventionally employ seismic methods to determine the source parameters. The approaches based on inversion of remote measurements of sea-level data have some advantages because seismic data are not available in short time after an event and are often imprecisely translated to tsunami data. Furthermore, tsunami wave propagation can be simulated more precisely than that of seismic waves.

Among the mathematical approaches based on inversion of near-field water-level data are the methods based on Green's functions technique (GFT) (Satake, 1987, 1989), least square inversion combined with the GFT (Tinti et al., 1996; Piatanesi et al., 2001) and an optimization approach (Pires and Miranda, 2001). A priori information from seismic data about a tsunami source played an essential role in the inversion method of Satake. One of the main advantages of the second methodologies is that it does not require a priori assumption of a fault plane solution. The first and the second approaches are based on the linear shallow water theory, but the third one allows using the nonlinear shallow water equations, or other appropriate equation sets. These methods have been widely applied in further studies of tsunami problem with various modifications (Wei et al., 2003) etc.

Among the recent studies dealing with the inverse tsunami source problem, it is necessary to cite an approach which is successfully applied now and which is a method of direct sorting combined with the minimal residual method (Percival et al., 2011; Lavrentiev et al., 2014). In brief, this method determines the unknown coefficients of a set of the typical unit tsunamigenic sub-faults disposed at the subduction zone so that residuals between the calculating data from such combination of unit sub-faults and the real DART^{R} data will be as small as possible in a least squares sense.

The developed numerical inversion technique based on least square inversion and truncated SVD approach is here described to reconstruct the initial tsunami waveform (*tsunami source*) in a tsunami source area based on inversion of remote water-level measurements (marigrams). This inversion method was first described in its fundamentals in Russian Scientific Journals (Voronina and Tcheverda, 1998; Voronina, 2004).

NHESSD
2, 7735–7772, 2014

Theoretical considerations of such a methodology for a linear long-wave model was discussed by Pires and Miranda (2001).

A direct problem of tsunami wave propagation is considered within the scope of the linear shallow-water theory. Numerical simulation is based on a finite difference algorithm on staggered grids. This ill-posed inverse problem of recovering initial tsunami waveforms is regularized by means of least square inversion using a truncated SVD approach. As a result of the numerical process, an r-solution is obtained (Cheverda and Kostin, 2010). The proposed method allows one to control the numerical instability of the solution and to obtain an acceptable result in spite of the so-called ill-posedness of the problem. The efficiency of the inversion is defined by the relative errors of tsunami source reconstruction. Analysis of the singular spectrum of a matrix obtained allows predict on a efficiency of inversion by using records produced at a given set of receivers.

One of the substantial advantage of this method is that it is completely independent of any particular source model and its distinguishing feature is a possibility to estimate the capability of a certain observation system to recover the tsunami source.

Basing on the properties of inverse operator studied numerically, we tried to answer the following questions: (1) what minimum number of marigrams should be used to reconstruct a tsunami source well enough, (2) where should the recorders (*receivers*) of the water-level oscillations be disposed relative to potential source area, (3) how accurately can a tsunami source be reconstructed based on recordings with a given monitoring system, (4) is it possible to improve the quality of reconstructing a tsunami source by distinguishing the *"most informative"* part of the observation system?

In order to answer these questions within the approach proposed, we have carried out a series of numerical experiments with synthetic data and different computational domain model. The results of the numerical simulations have shown a promising outlook of this approach.

NHESSD
2, 7735–7772, 2014

2 Models

Mathematically, the problem of recovering the initial tsunami waveform in a source area is formulated as the determination of the spatial distribution of an oscillation source using remote measurements on a finite set of points (later called *receivers*). Let us consider a coordinate system xyz and direct the axis z downwards. The plane $\{z = 0\}$ corresponds to an undisturbed water surface. The curvature of the Earth is neglected. Consider the aquatic part Φ of a rectangular domain $\Pi = \{(x;y) : 0 \le x \le X; 0 \le y \le Y\}$ on the plane $\{z = 0\}$ with solid boundaries Γ and straight-line sea boundaries. The interaction between the wave and the coast is not considered in this study. Our numerical model is based on the shallow water theory. On addition, we look for a solution only in a constrained region. The source area is assumed to be known from seismological data.

Let $\Omega = \{(x,y) : x_1 \le x \le x_M; y_1 \le y \le y_N\}$ be a tsunami source subdomain of Φ. Let $\eta(x,y,t)$ be a function of the water surface elevation relative to the mean sea level. This function is considered to be a solution of the linear shallow water equation:

$$\eta_{tt} = \mathrm{div}(gh(x,y)\mathrm{grad}\eta) + f_{tt}(x,y,t) \quad (1)$$

with the initial conditions:

$$\eta_{|t=0} = 0; \quad \eta_{t|t=0} = 0 \quad (2)$$

with the completely reflecting conditions on the continental coasts:

$$\left.\frac{\partial \eta}{\partial n}\right|_{\Gamma} = 0. \quad (3)$$

Fully absorbing boundary conditions (ABC) (Enquist and Majda, 1977) of second order accuracy are implied on the open boundaries. The acceleration of gravity is denoted as g and the wave phase velocity is defined as $c(x,y) = \sqrt{gh(x,y)}$. The tsunami wave

NHESSD
2, 7735–7772, 2014

is assumed to be triggered by a sudden vertical displacement $f(x,y,t)$ of the sea floor. It is assumed that

$$f(x,y,t) = H(t)\varphi(x,y),$$

where the function $\varphi(x,y)$ is a co-seismic vertical displacement and $H(t)$ is the Heaviside step function. As a result the function $\varphi(x,y)$ is the initial sea surface deformation in the target domain Ω. The variable $h(x,y)$ is the water depth relative to the mean sea level.

The set-up inversion experiments are substantially different in the function $h(x,y)$ which varies from $h(x,y) = \text{const}$ to a special $h(x,y) = h(x)$ modeling the shelf zone and, finally, to the real bathymetry of a Peru subduction zone.

The observational data are water level records which are assumed to be known at a set of points $M = \{(x_i,y_i), i = 1,\ldots,P\}$ in the domain Φ:

$$\eta(x_i,y_i,t) = \eta_0(x_i,y_i,t),\ (x_i,y_i,) \in M. \tag{4}$$

One can also assume that the set of points M belongs to some line γ without self-crossing in the domain Φ that is necessary only for theoretical purposes.

3 Inversion method

In short, this method is as follows. Let us denote by A the linear operator of the Cauchy problem presented by Eqs. (1)–(3) and trace its solution on the line $\gamma(s)$. Under an appropriate assumption on the functions $h(x,y)$, $\varphi(x,y)$ and the line $\gamma(s)$ (this assumption does not necessarily hold in the experiments), by means of the standard technique of embedding theorems it was proved (Voronina, 2004, 2012) that the operator $A : L_2(\Omega) \to L_2(\gamma(s) \times (0,T))$ is compact and, therefore, does not possess a bounded inverse. Thus, Eqs. (1)–(3) are now reduced to the following equation:

$$A\varphi = \eta_0(s,t), \tag{5}$$

NHESSD
2, 7735–7772, 2014

where

$$\eta_0(s,t) = \eta(x(s),y(s),t), \quad (x(s),y(s)) \in \gamma(s),$$
$$0 \le t \le T, \quad 0 \le s \le L.$$

As was shown by Kaistrenko (1972), the above inverse problem has a unique solution only if the source function allows factorization in the temporal and spatial variables.

The inverse problem in question can now be formulated as the problem of solving a linear operator equation of the first kind. Its solution will be sought for in a least squares formulation. In other words, any attempt to numerically solve Eq. (5) must be followed by a certain regularization procedure. In the present study, regularization is performed by means of truncated SVD that brings about a notion of r-solution (Cheverda and Kostin, 2010).

In brief, the notion of r-solution can be described as follows. Any compact operator A can be described in a Hilbert spaces with a singular system $\{s_j, \boldsymbol{u}_j, \boldsymbol{v}_j\}$, $j = 1, \ldots \infty$, where $s_j \ge 0$ ($s_1 \ge s_2 \ge \ldots \ge s_j \ge \ldots$) are singular values and $\{\boldsymbol{u}_j\}$, $\{\boldsymbol{v}_j\}$ are the left and the right singular vectors. $A\boldsymbol{v}_j = s_j \boldsymbol{u}_j$ and $s_j \to 0$ with $j \to \infty$. The systems $\{\boldsymbol{u}_j\}$, $\{\boldsymbol{v}_j\}$ are orthogonal. A very important property of the singular vectors is that they form bases in the data and model spaces, therefore, the solution of Eq. (5) can be given by the expression:

$$\varphi(x,y) = \sum_{j=1}^{\infty} \frac{(\eta_0(s,t) \cdot \boldsymbol{u}_j)}{s_j} \boldsymbol{v}_j(x,y). \tag{6}$$

As one can see from Eq. (6), the ill-posedeness of the operator equation of the first kind with compact operator is due to the fact that $s_j \to 0$ with $j \to \infty$, i.e. one can perturb the right-hand side $\eta_0(s,t)$ in such a way, that its vanishing perturbation can lead to a large perturbation of the solution.

NHESSD
2, 7735–7772, 2014

The regularization procedure based on truncated SVD leads to a notion of r-solution given by the relation:

$$\varphi^{[\mathbf{r}]}(x,y) = \sum_{j=1}^{r} \frac{(\eta_0(s,t)\cdot \boldsymbol{u}_j)}{s_j} \boldsymbol{v}_j(x,y). \tag{7}$$

An r-solution is the projection of the exact solution of Eq. (6) onto a linear span of r right singular vectors corresponding to the top singular values of the compact operator A. This truncated series is stable for any fixed parameter r with respect to perturbations of the right-hand side and the operator as it is (Cheverda and Kostin, 2010). The value of r is determined by the relation

$$r = \max\{k : s_k/s_1 \geq 1/\mathrm{cond}\}, \tag{8}$$

where cond = cond($\mathbf{A}$) is setting by the user restriction on the conditioning number of the matrix $\mathbf{A}$. It is clear, the value of r depends on the rate of decreasing of singular spectrum of the matrix $\mathbf{A}$, which is tightly bounded with the parameters of the observation system, and noisiness of data. Indeed, let us assume the perturbation in the right-hand side $\boldsymbol{\eta}_0(s,t)$ is known and can be written in the form

$$\boldsymbol{\varepsilon}(t) = \sum_{j=1}^{L} \varepsilon_j(t)\boldsymbol{u}_j,$$

then the perturbed solution will be represented, respectively as

$$\varphi^{[r]}(x,y) = \sum_{j=1}^{r} \frac{(\eta_{0j}(s,t) + \varepsilon_j(t))}{s_j} \boldsymbol{v}_j(x,y). \tag{9}$$

One should limit the upper index in the last sum from the time when s_j is far less $\varepsilon_j(t)$ to avoid the numerical instability. It is reasonable that the larger r, the more informative

NHESSD
2, 7735–7772, 2014

the solution. Note, the fitted value of r is much less than a minimum of the matrix dimensions.

The analysis of the singular spectrum of the matrix **A** is the key aspect in the proposed methodology because it allows one to predict the efficiency of the inversion with a certain observation system and bathymetry.

4 Finite dimensional approximation and r-solution

In a real situation, one can numerically resolve only a finite dimensional subsystem of Eq. (5) with $(L \times K)$ submatrix. Convergence of the r-solution of a finite-dimensional system of linear algebraic equations to the r-solution of an operator equation was carefully investigated in Cheverda and Kostin (2010).

To solve numerically Eqs. (1)–(3) we applied a finite difference approach for its equivalent first order linear system in terms of the unknown water elevation $\eta(x,y,t)$ and velocity vector $\boldsymbol{v}$:

$$\eta_t + g\nabla\cdot(h\boldsymbol{v}) = 0 \tag{10}$$

$$\boldsymbol{v}_t + g\nabla\eta = 0 \tag{11}$$

completed by the following initial conditions:

$$\eta|_{t=0} = \varphi(x,y), \qquad \boldsymbol{v}|_{t=0} = 0; \tag{12}$$

and the boundary condition on the solid boundary:

$$\boldsymbol{v}\cdot\boldsymbol{n} = 0 \tag{13}$$

and free path conditions on the open boundaries. This problem was approximated by an explicit-implicit four-point finite difference scheme on a uniform rectangular grid which is based on the staggered grid stencil using the central-difference approximation

NHESSD
2, 7735–7772, 2014

of spatial derivatives. As it was mentioned above, the wave run up is not considered in this study, hence we infer the coast line when the depth $h(x,y) = 50\,\text{m}$.

In order to obtain a system of linear algebraic equations by means of the projective method, a trigonometric basis was chosen in the model space, i.e., the unknown function of water surface elevation $\varphi(x,y)$ is approximated in the target domain Ω (Section Models) by a sum of spatial harmonic $\{\varphi_{mn}(x,y) = \sin\frac{m\pi}{l_1}x \cdot \sin\frac{n\pi}{l_2}y\}$ with unknown coefficients $\boldsymbol{c} = \{c_{mn}\}$:

$$\varphi(x,y) = \sum_{m=1}^{M}\sum_{n=1}^{N} c_{mn}\varphi_{mn}(x,y), \tag{14}$$

the center of the tsunami source was believed to be at a point (x_c, y_c) being the central point of the domain Ω and $l_1 = (x_M - x_1)$; $l_2 = (y_N - y_1)$. We assumed the water level oscillations $\boldsymbol{\eta_0}(x,y,t)$ are known at a set of points $\{(x_p,y_p)\}$, $p = 1,\ldots,P$ for a finite number of time $\{t_j\}$, $j = 1,\ldots,N_t$, i.e.

$$\boldsymbol{\eta_0} = (\eta_{11},\eta_{12},\ldots,\eta_{1N_t},\eta_{21},\ldots,\eta_{2N_t},\eta_{P1},\ldots,\eta_{PN_t})^T,$$
$$\eta_{pj} = \eta_0(x_p,y_p,t_j).$$

The unknown function $\varphi(x,y)$ was sought for according to Eq. (14).

Now, we assume that the dimensions of the solution and the data space are equal to: $\dim(\text{sol}) = K = M \times N$; $\dim(\text{data}) = L = P \times N_t$. In the end, a linear algebraic system for the unknown vector $\boldsymbol{c}$ of coefficients $\{c_i\}$ from Eq. (14) was obtained:

$$\boldsymbol{\eta}_0 = \mathbf{A}\boldsymbol{c}, \tag{15}$$

where $\mathbf{A}$ is a matrix whose columns consist of computed waveforms in every receiver for each spatial harmonic used as the source, $\boldsymbol{\eta}_0$ is a vector containing the observed tsunami waveforms. Now, the matrix $\mathbf{A}$ is a rectangular one with K colums and L rows.

NHESSD
2, 7735–7772, 2014

After the SVD (singular value decomposition) procedure one could obtained the singular values of the matrix **A**, its left and right singular vectors $\{\mathbf{u}_i,\ i = 1,\ldots,L\}$,$\{\mathbf{v}_k, k = 1,\ldots,K\}$. The value r could be fitted by analyzing the singular spectrum of the matrix **A**.

Then the r-solution of Eq. (15) is represented by the sum

$$\boldsymbol{c}^{[r]} = \sum_{j=1}^{r} \alpha_j \boldsymbol{v}_j, \tag{16}$$

where $\{\alpha_j = \frac{(\boldsymbol{\eta}_0, \boldsymbol{u}_j)}{s_j}\}$ and $\{\boldsymbol{u}_j\}$, $\{\boldsymbol{v}_j\}$ are the left and the right singular vectors of the matrix **A**, $\{s_j\}$ are its singular values.

Finally, the numerical simulation includes the following steps:

1. First, we obtain synthetic marigrams in all receivers by solving the forward problem with a certain function $\varphi(x,y)$ as a source to be reconstructed. Thus, the vector $\boldsymbol{\eta}_0(x,y,t)$ in Eq. (15) is obtained.
2. The computed marigrams are perturbed by a background noise, i.e., a high-frequency disturbance and appropriate filtering is applied.
3. Next, the matrix **A** is numerically computed by solving the forward problem with every spatial harmonic $\{\varphi_{mn}\}, m = 1,\ldots,M; n = 1,\ldots,N$ as a source.
4. Further, the standard SVD- procedure is applied. The analysis of singular spectrum of the matrix **A** allows one to choose the number r varying the conditioning number of the matrix **A**, as was explained above, and to compute the coefficients $\{c_{mn}\}$ by solving Eq. (15).
5. After this, the function $\varphi(x,y)$ can be computed in the form according Eq. (14).
6. To estimate the efficiency of the inversion experiment we use a misfit parameter that represents the squared averaged difference between the exact solution function $\{\varphi_i = \varphi(x_i, y_i)\}$ and the recovered one $\{\hat{\varphi}_i = \hat{\varphi}(x_m, y_n)\}$:

NHESSD
2, 7735–7772, 2014

$$\text{err}\% = \left(\frac{\sum_{i=1}^{K} (\varphi_i - \hat{\varphi}_i)^2}{\sum_{i=1}^{K} (\varphi_i)^2} \right)^{1/2} \times 100\,\%,$$

where $i = n + (m-1) \times N; n = 1, \ldots, N; m = 1, \ldots, M; K = N \times M$. Bellow, the misfit parameter is denoted by err%.

5 Numerical experiments: description and discussion

A series of calculations have been carried out by the method proposed to clarify the dependence of the efficiency of the inversion on certain characteristics of the observation system such as the number of receivers and its location, frequency or temporal range of data and the signal-to-noise ratio. We believe that source area Ω is given, as it is in real cases. Synthetic data for the numerical inversion experiments presented below were computed as a solution of Eqs. (11)–(13) with respective open boundary conditions. In addition, the function $\varphi(x,y)$ was explained by the relation:

$$\varphi(x,y) = \beta(x,y) \cdot \alpha(x), \tag{17}$$

where function $\beta(x,y)$ makes a semi-paraboloid with the center at the point (x_0, y_0) and the radii R_x and R_y on the plane $z = 0$; the parameter $\alpha(x)$ is perturbation of this semi-paraboloid $\beta(x,y)$ and was set up as $\alpha(x) = 1$ when the initial tsunami waveform was assumed to be a semi-paraboloid or a semi-sphere.

5.1 Case study $h(x,y) = \text{const}$

First, to avoid the influence of such factors as bathymetry and data noise, we consider a formal calculation domain with open boundaries, with the depth $h(x,y) = h_0$, the wave

NHESSD
2, 7735–7772, 2014

phase velocity $c(x,y) = \sqrt{gh_0} = c_0$ and $\alpha(x) = 1$. The setting of the problem allows to consider our problem in the spectral domain and to use the r-solution method for analytical solution (Voronina and Tcheverda, 1998; Voronina et al., 2014). The basic properties of inverse operator were numerically studied.

In short, we have shown that the inversion results are better when the aperture length is rising, increasing the upper limit of the frequency band makes the obligatory effect for the inversion quality and leads to decreasing the "smearing" of the recovered function and, hence, to increasing an extreme values in the center of the source. The results of the inversion by a wide angle aperture coincide with the experiments on a wide linear aperture. It was shown, if receivers were uniformly distributed along the linear aperture, the efficiency of the inversion was improving when the number of receivers increases up to 15 but further increasing the receivers number was useless. A receivers-to-source distance has no affects on on the inversion result in the case studied. If the number of receivers is fixed the efficiency of the inversion rises with the azimuthal coverage. We have shown that a more precise definition of the target domain relative to the size of a tsunami source leads to decreasing the number of necessary receivers, perhaps as little as 5–7 ones. In addition, the released energy is increasing as well as a maximum value of the recovered function. However, the total volume of water displaced due to the source in the domain Ω is not varied.

The results obtained allowed us to outline the main details of the methodology proposed. The basic point is that analyzing a singular spectrum of the obtained matrix **A** enables us to make an assumption about the forthcoming efficiency of the inversion.

Let us see how that works in the context of the dependence the efficiency of the inversion on the number of receivers and their azimuthal coverage. Our numerical experiments were conducted with the following parameters: $\Omega = \{(x,y) : -100 \le x \le 100; 100 \le y \le 200\}$, $w \in [0.001, 0.01]$ Hz; $\alpha(x) = 1$ in Eq. (17), i.e. the type of the source is a semi-ellipsoid with $R_x = 50$; $R_y = 25$ and the center was assumed at the point (0,150) (all dimensions are given in km). The conditioning number of the matrix **A** was 10^8 in all calculations.

NHESSD
2, 7735–7772, 2014

Our purpose was to obtain acceptable results of the inversion using a minimum of marigrams, so, we made a computer simulation when the number of receivers ranged from 1 to 5 and they were placed on the circle with radius $R = 150$ and center at point (0,150). Figure 1 (left) shows a layout scheme of the source-receivers arrangement.

We will use the following notations: (1) the conditioning number of the matrix **A** is designated as cond(A), (2) the value $100 \times \max(\varphi(x,y))$, while $(x,y) \in \Omega$ is denoted by the symbol $\{100\max\}$, (3) the misfit parameter is denoted by err%.

The common logarithms of singular values for these numerical experiments are plotted in Fig. 1 (middle). *A sharp decrease in the singular values, when their number increases, is typical for all calculations in all cases of the study, due to the ill-posedness of the problem*.

Comparing the singular spectra in Fig. 1 (middle) we can believe the worse result of inversion when 1–2 receivers were used, while the best result is provided by using 5 receivers. Moreover, the behavior of singular spectra makes it possible to expect the improvement of inversion with increasing the aperture angle for every set of receivers.

It is also shown in Fig. 1 (middle), how one could define the number r for every settled conditioning number of the matrix **A**.

As will be clear below, only increasing the number of records does not lead to a good inversion if there is no sufficient azimuthal coverage with respect the source and, on the contrary, in real cases it turns out that the noisiness of data is raised resulting in lowering the efficiency of inversion.

Indeed, in Fig. 1 (right) one can see how the number r (the blue line) and a maximum value of the recovered function (the red line) varied on the number of receivers used (the horizontal axis) and aperture angle (the green line). One can see from this graphs, increasing the number of receivers, in total, leads to a worse inversion: misfit parameter (the orange line) is decreasing with increasing the number of receivers used, as well as maximum value of the recovered function tends to a maximum value of the theoretical function. If the number of receivers is fixed, the efficiency of inversion rises with the azimuthal coverage that has a good matching with our previous assumption

NHESSD
2, 7735–7772, 2014

based on analyzing singular spectra. We have also shown that if the aperture angle is sufficiently wide, the influence of the conditioning number is not significant, but the inversion parameters are worse for a smaller conditioning number of the matrix **A**. The recovered functions for the above a discussed cases are presented in Figs. 2 and 3.

5.2 Case study $h(x,y) = h(x)$

How a bottom relief and a more realistic type of the source influence the inversion result? To answer this question we have carried out numerical experiments for the model bottom topography having some basic morphological features typical of the island arc regions (Fig. 4, left).

As the initial sea surface displacement, a sea floor deformation of typical tsunamigenic earthquakes with reverse dip-slip or low-angle trust mechanisms was used. Its dipolar shape was simulated according to Eq. (17) with the parameter $\alpha(x) = (x - x_0 + 3 \times R_1) \times (x - x_0 + R_1/6)$; and $R_1 = 25$; $R_2 = 50$ (see Fig. 4, middle left). The target domain Ω was a rectangle $\{(x,y) : \in [100;200] \times [50;150]\}$, the calculation domain was a rectangle $\Pi = \{(x,y) : \in [0;300] \times [0;200]\}$, the center point of the tsunami source was placed at $(x_0;y_0) = (150;100)$.

Synthetic data for the numerical inversion experiments presented below were computed as a solution of Eqs. (11) and (12). The full reflection boundary condition described in Eq. (13) is fulfilled on the coast line $x = 0$ and the absorbing boundary conditions are imposed on the open free boundaries:

$$c\eta_{yt} + \eta_{tt} + \frac{c^2}{2}\eta_{xx} = 0, \ (x,y) \in y = 0;$$

$$-c\eta_{yt} + \eta_{tt} + \frac{c^2}{2}\eta_{xx} = 0, \ (x,y) \in y = 200;$$

$$-c\eta_{xt} + \eta_{tt} + \frac{c^2}{2}\eta_{yy} = 0, \ (x,y) \in x = 300.$$

NHESSD
2, 7735–7772, 2014

The function $\varphi(x, y)$ was sought for according to Eq. (14) with $M = 25$, $N = 11$. Synthetic marigrams were calculated for $N_t = 1990$ time instants. Receivers were disposed on the segment [10; 190] of the line $x = 0$, i.e. a maximum of the aperture length was 180.

As in the previous case with constant a depth of the calculated basin we tried to use a minimum number of marigrams in the inversion process. For this reason, the parameter P was equal to 1, 2, 3, 5. Some aspects of this study were presented in Voronina (2004). We now turn to these models to make a generalization. The point in question is the location of receivers with respect to the dipolar source.

At the initial stage, the numerical experiments were made without noisy data. Let us name the central point of our linear aperture as a *midpoint*. By the *midpoint* we mean the projection of the central point of the rectangle Ω (or the central point of the source, what is the same) onto the aperture line.

The graphs of the misfit parameter err% when one (the blue line) and two (the pink line) receivers were used in terms of the position of receivers on the aperture line (horizontal axis) are plotted in Fig. 5. There is an aperture length on the horizontal axis in Fig. 5. It should be noted that the aperture line is the axis-Y and coordinates of receivers are $(0, 10n)$, the value n is a coefficient of the aperture length $10n$, $n = 1, \ldots, 19$.

The most important information that should be drawn from these graphs points up the presence of an obvious minimum of the functions presented. One can see points of a minimum in these graphs corresponding to the experiments with the receiver disposed at *midpoint*. In other words, availability of marigram from this observation point significantly improves the inversion result. The following numerical experiments are confirmed this inference.

The misfit parameter plotted in Fig. 5 (left) (the pink line) refers to the following numerical experiments with two receivers: the first receiver was fixed at the initial point of the aperture and the second one was moving to the endpoint of the aperture segment stopping every 10 km.

NHESSD
2, 7735–7772, 2014

A substantial decrease of the misfit parameter when receivers are placed at the *midpoint* can be explained by the dipolar shape of the source and, hence, the signal in this direction is mostly informative.

For this reason, in the following experiments with three and five receivers, one of receivers is always fixed at the *midpoint*. The conditioning number of the matrix **A** was equal to 100 in the experiments below.

Later, synthetic marigrams were simulated as a result of the solution to the direct problem described in Eqs. (11)–(13) perturbed by the background noise, it was a high-frequency disturbance about 5 % rate of a maximum signal amplitude over all the receivers. Admittedly, we did not obtain any appropriate result with perturbed synthetic data due the ill- posedness of the problem. However, since a tsunami wave is more lower-frequency as compared to the background noise, it is reasonable to apply the frequency filtration of an observation signal. In this paper, filtration is done by a method of grid function smoothing proposed by V. A. Tsetsoxo and A. S. Belonosov (Yurchenko et al., 2013).

The graphs in Fig. 5 (middle) show that a higher rate of the synthetic background noise results in increasing the misfit parameter with the same conditioning number of the matrix **A** in spite of filtration. It is clear from graphs in Fig. 5 (right), that increasing the conditioning number of the matrix **A** allows one to use a larger value r and, therefore, to obtain a more precise solution and a lesser misfit parameter.

We have considered the following versions of the receivers disposition:

Case (1). An observation system of three receivers. One receiver is always placed at the *midpoint* but two other receivers are symmetrically placed with respect to the *midpoint* with distances $10n, n = 1, \ldots, 9$ every step.

Case (2). An observation system of five receivers. Again, one receiver is always placed at the *midpoint*, two pairs of receivers moved symmetrically from the center to the endpoints of the aperture, while a distance between every nearest-neighbor receivers in every pair was fixed as 40 km (the case named C2.1), 20 km (the case named C2.2) and 10 km (C2.3).

NHESSD
2, 7735–7772, 2014

From the graphs of singular spectra of the inversions with three and five marigrams plotted in Fig. 6 (left) one can expect that the inversion in the latter case will be more successful. Indeed, the numerical experiments (see Fig. 6, right) substantiate our assumption based on analyzing singular spectra.

There is an aperture length on the horizontal axis in Fig. 6 (middle–right). The parameters of the inversion for Case (1) as a functions of the aperture length are presented in Fig. 6 (middle). The misfit parameter err% (the blue line) is decreasing but maximum and minimum values of the recovered function (the orange and the green lines, respectively) converge to the corresponding values of the initial function (the red lines) at the moment when the aperture length approaches the projection of a source on the aperture line that corresponds to the yellow columns in Fig. 6 (middle).

These regularities remain valid for the inversion with five marigrams (see Fig. 6, right). It is notable, that the misfit parameters and a maximum value of the recovered function in the inversion using five marigrams in case C2.2 (the violet and the green lines) are better than the one that was made by using three marigrams (the blue and the pink lines). The misfit parameter in case C2.3 (the red line) is plotted, too. Case C2.2 differs from case C2.3 by a more uniform distribution of the same number of receivers within the acting aperture segment being the projection of the source on the aperture line that leads to improving the inversion parameters.

By comparing the values of parameters in the yellow and light-blue columns in Fig. 6 (middle-right) one can conclude that a further increase in the aperture length leads to worse results.

The importance of the receiver location at the *midpoint* was confirmed in these series of the numerical experiments, too. As was shown, replacing the central point of a set of receivers from the *midpoint* results in increasing the misfit parameter and, at the same time, in decreasing the maximum value of the recovered function. In other words, we lose the most informative marigram.

As an example, the recovered functions corresponding to the inversion for Case (1) and Case (2.2) are presented in Fig. 4 (middle right and right).

NHESSD
2, 7735–7772, 2014

It is now clear that the quality of inversion strongly depends on the disposition, the number of receivers and noisy data. The robust result could be obtained when, at least, one of the receivers involved is placed at the *midpoint* which is a projection of the major variability direction of the source.

5.3 Case study: real bathymetry of the Peru subduction zone

Finally, to illustrate some of the ideas let us consider the results obtained for the case study with the real bathymetry of a Peru subduction zone. We were interested, how distinctive features of a real bathymetry affect the inversion process.

We set up the following parameters for our calculations: the domain Φ was the aquatic part of a rectangle $\Pi = \{0 \le x \le 600; 0 \le y \le 400\}$ with piecewise-linear boundaries of the dry land, the domain $\Omega = \{400 \le x \le 500; 200 \le y \le 300\}$ (see Fig. 7). As was mentioned above, the wave run up was not considered. The observed data were simulated as a result of solution of Eqs. (11)–(13) completed with the full absorbing boundary conditions of second order of accuracy being fulfilled on the open boundaries.

Again, as an initial sea surface elevation, the sea floor deformation of typical tsunamigenic earthquakes with reverse dip-slip or low-angle trust mechanisms was used and it is plotted in Fig. 11 (left) with the parameters: the center point $(x_0; y_0) = (450; 250)$, maximum and minimum values of initial displacement in source area $\varphi(x, y)$ $\varphi_{\max} = 1.959\,\mathrm{m}$; $\varphi_{\min} = -0.67\,\mathrm{m}$.

As before, we tried to obtain acceptable results of the inversion using a minimum number of records.

In our calculations, the function $\varphi(x, y)$ was sought for according to Eq. (14) with $M = 25$, $N = 11$. These values are defined by the shape of theoretical function $\varphi(x, y)$. Depth $h(x, y)$ was assumed to be a real bathymetry of the Peru subduction zone. We placed 14 receivers at points in the domain Φ which are enumerated according to Fig. 7 and are marked by the green color (∘), i.e., $P = 14$ in Eq. (4). A time interval was

NHESSD
2, 7735–7772, 2014

extent enough for the tsunami wave to reach all receivers, specifically, the number of time steps was N_t = 1684 in the case presented.

After specifying all the parameters, we consequently carried out the steps of the numerical simulation mentioned in Sect. 4. Synthetic marigrams were perturbed by the background noise with the disturbance rate about 3% of a signal maximum amplitude over all the receivers. It is imperative that the filtration procedure was made after the noise pollution. Next, the standard SVD-procedure was performed and the singular spectrum of the matrix **A** was obtained.

As before, first of all we analyzed singular spectrum of the matrix **A**. For example, the graphs of the common logarithm of the singular values of the matrix **A** corresponding to their numbers are presented in Fig. 8. for the inversion with three (the red line), four (the blue line), nine (the magenta line) and ten (the green line) marigrams used in the calculations. Comparing singular spectra for the inversion with some sets of three and four marigrams in Fig. 8, one can assume that such an increase in the number of receivers will lead to the deterioration of the solution. Inversion parameters corresponding to these cases are presented in Table 1 (the first and the fifth rows).

We have seen, until now, that adding new receivers had always led to better solutions when a depth of the calculation basin was a simulative function. However, this prediction is not universally true for the case with a real bathymetry. Only increasing the number of receivers without considering their azimuthal coverage could result in a worse inversion due to rising a general level of noise pollution of data.

Obviously, the parameter r should be taken only from the first interval, where the common logarithms of singular values are slightly sloping, because, further increase in number r leads to the solution instability. On the other hand, r should be large enough to provide a suitable spatial approximation of $\varphi(x, y)$. From the numerical experiments it is clear that a satisfactory parameter value has to $r \geq 70$ (Voronina, 2011).

Some results of our numerical simulations confirming these inferences are presented in Table 1. Analyzing the values of the inversion parameters in Table 1, one can see

NHESSD
2, 7735–7772, 2014

that the inversion with five marigrams (the eighth row) is better than the inversion with nine or ten marigrams (the 11th, 12th, 14th and 15th rows).

Comparing the inversion parameters in Tables 1 and 2 one has to look at Fig. 7. It is clear that the key role in improving the quality of the inversion played by appears the location of the monitoring system relative to the topography features and source area.

Indeed, adding to the observation system the receivers with numbers $\{12, 13, 14\}$ (see the 12th and the 15th rows in Table 1) which were not affected by disturbance due to the reflection from the underwater vertical ledge, did not improve the solution, according to the expectations. The same is true for a set of receivers $\{1, 2, 3, 4\}$ which, on the contrary, were placed in the direction where the distortion of the signal is more possible due to the features of the relief. Using receivers with numbers $\{5, 6, 7, 8, 9, 10, 11\}$ one can obtain a strong improvement of the inversion. The replacement of even one-two of them leads to a solution deterioration (see the third and the fourth rows in Table 2). What's the odds? It seems reasonable to say that the matter is in the dipole shape of our source and in the existence of a certain angle between its axis and the line of the reflection (the coast line and the underwater ledge). The axis of the source in our case is directed along the axis X and is not perpendicular to the coast line like in the previous model. The latter set of receivers is distributed along the reflection ray corresponding to the direction of the strongest variability of the source. It should be remarked that the use of all the receivers does not improves the inversion because this set of marigrams involves many fewer informative waveforms that only leads to increasing the noisy pollution of the data.

The last series of the numerical experiments were aimed at finding out the most informative direction of the receivers location in terms of improving the inversion. We have chosen several sets each consisting of seven receivers differing in their location.

The upper parts of singular spectra for these numerical experiments with cond($\mathbf{A}$) = 100 (the green horizontal line) and cond($\mathbf{A}$) = 1000 (the red horizontal line) are plotted in common logarithm scale in Fig. 9.

NHESSD
2, 7735–7772, 2014

In Table 2 one can see the major parameters of the inversion with seven marigrams by Models V1–V4 which differ in the receivers location and the conditioning number of the matrix **A**.

The recovered functions for models V1.1, V2.1, V3.1, V1.2, V2.2, V3.2 are plotted in Fig. 11. It is clear, the use of the large conditioning number of the matrix **A** and, as consequence, a large value of r in the liable interval leads to a lesser smearing effect in the shape of the recovered function.

It should be noted that the misfit parameter gives only a global estimation of the efficiency of the inversion. Based on our experiments with perturbed data and a real bathymetry we can conclude that the value of the misfit parameter err% $\approx$ 20–26 % allows us to obtain a robust shape of the recovered source.

In Fig. 11 the theoretical function $\varphi(x, y)$ and the recovered by model V3.2 one are presented. The extreme values of the recovered function have changed due to smoothing.

After the inversion by model *V*3.2 was completed, we again solved the direct problem with the recovered and smoothed function $\hat{\varphi}(x, y)$ and calculated marigrams at the same 14 points. Marigrams computed with the recovered tsunami source have a good matching with the initial synthetic ones not only in seven receivers used in the inversion process but also in all 14 receivers as well (Voronina, 2012).

This fact can be treated as a verification of the inversion algorithm. In addition, the coincidence of marigrams has a great importance for predicting water elevation in the area relying on data provided by some monitoring system.

6 Conclusions

We have applied an approach based on SVD and r-solution methods to recovering the initial tsunami waveform in a tsunami source area.

Searching for the initial water surface displacement as a series of spatial harmonics is a common practice however the method proposed allows one to control the numer-

NHESSD
2, 7735–7772, 2014

ical instability by tools of the r-solution method. The value r is essentially determined by a real bathymetry, spatial location of the observation system, the data noisiness and still it is significantly less than the dimension of the matrix. By analyzing the singular spectrum of the matrix obtained in the calculations it is possible to make a preliminary prediction of the efficiency of the inversion with a given set of the recording stations. Hence, we could make a well-aimed precomputation with a varying location of candidate receivers to obtain the best inversion in possibly a real process. This potential of the method should be kept in mind when designing a monitoring system for tsunamis.

By the numerical simulations we have shown that in order to obtain a reasonable quality of the source restoration we need at least five- seven receivers in the simulation with a real bathymetry. Reconstructing the shape of a source is improved when not only the number of receivers increases but their azimuthal coverage with respect to a source area is improving as well. A receivers-to-source distance does not essentially influence the inversion result. One of the advantages of the method proposed is that it is completely independent of any particular shape of a source, however, a limitation of this method is that it is suitable only for the linear theory.

The location of receivers on direct and reflected rays corresponding to the direction of the strongest variability of the dipole source have the greatest effect for the inversion result. As is shown in the numerical experiments, it is this set of receivers provides the best result of the inversion process.

Acknowledgements. The research was supported by Russian Foundation for Basic Research grants No 12-07-00406, by the Siberian Branch of the RAS (Project 117) and the Far-East Branch of the RAS (Project 37).

NHESSD
2, 7735–7772, 2014

References

Cheverda, V. A. and Kostin, V. I.: r-pseudoinverse for compact operator, Siberian Elect. Math. Rep., 7, 258–282, 2010. 7738, 7741, 7742, 7743

Enquist, B. and Majda, A.: Absorbing boundary conditions for the numerical simulation of waves, Math. Comp., 139, 629–654, 1977. 7739

Kaistrenko, V. M.: Inverse problem for reconstruction of tsunami source, Tsunami Waves. Proc. Sakhalin Compl. Inst., 29, 82–92, 1972. 7741

Lavrentiev, M. M. and Romanenko, A. A.: Tsunami wave parameters calculation before the wave approaches coastal line, in: Proceedings of the Twenty-fourth (2014) International Ocean and Polar Engineering Conference, Busan, Korea, 15–20 June, 1098–6189, 3, 96–102, 2014. 7737

Percival, D. B., Denbo, D. W., Eble, M. C., Gica, E., Mofjeld, H. O., Spillane, M. C., Tang, L., and Titov, V. V.: Extraction of tsunami source coefficients via inversion of DARTr buoy data, Nat. Hazards, 58, 567–590, 2011. 7737

Piatanesi, A., Tinti, S., and Pagnoni, G.: Tsunami waveform inversion by numerical finite-elements Green's functions, Nat. Hazards Earth Syst. Sci., 1, 187–194, doi:10.5194/nhess-1-187-2001, 2001. 7737

Pires, C. and Miranda, P. M. A.: Tsunami waveform inversion by adjont methods, J. Geophys. Res., 106, 19773–19796, 2001. 7737, 7738

Satake, K.: Inversion of tsunami waveforms for the estimation of a fault heterogeneity: method and numerical experiments, J. Phys. Earth, 35, 241–254, 1987. 7737

Satake, K.: Inversion of tsunami waveforms for the estimation of hereogeneous fault motion of large submarine earthquakes: the 1968 Tokachi-oki and the 1983 Japan sea earthquake, J. Geophys. Res., 94, 5627–5636, 1989. 7737

Tinti, S., Piatanesi, A., and Bortolucci, E.: The finite-element wavepropagator approach and the tsunami inversion problem, J. Phys. Chem. Earth, 12, 27–32, 1996. 7737

Voronina, T. A.: Determination of spatial distribution of oscillation sources by remote measurements on a finite set of points, Sib. J. Calc. Math., 3, 203–211, 2004. 7737, 7740, 7750

Voronina, T. A.: Application of r-solutions to reconstructing an initial tsunami waveform, Numer. Meth. Program., 14, 165–174, 2013.

Voronina, T. A.: Reconstruction of initial tsunami waveforms by a trancated SVD method, J. Inverse Ill-Pose. P., 19, 615–629, 2012. 7740, 7756

NHESSD
2, 7735–7772, 2014

Voronina, T. A. and Tcheverda, V. A.: Reconstruction of tsunami initial form via level oscillation, Bull. Nov. Comp. Center, Math. Model. Geoph., 4, 127–136, 1998. 7737, 7747
Voronina, T. A., Tcheverda, V. A., and Voronin, V. V.,: Some properties of the inverse operator for a tsunami source recovery, Siberian Electronic Mathematical Reports, available at: http://semr.math.nsc.ru, last access: 11 November 2014, 532–547, 2014. 7747
Wei, Y., Cheung, K. F., Curtis, G. D., and McCreery, C. S.: Inversion algorithm for tsunami forecast, J. Waterw. Port Coastal Ocean Eng., 129, 60–69, 2003. 7737
Yurchenko, M. A., Belonosova, A. V., and Belonosov, A. S.: On an algorithm to solve an inverse kinematic problem of seismics: Siberian Electronic Mathematical Reports, available at: http://semr.math.nsc.ru, last access: 5 December 2014, 74–86, 2013. 7751
Zuhair Nashed, M.: Aspects of generalized inverses in analysis and regularization, in: Generalized Inverses and Applications, Academic Press, New York, 193–244, 1976.

NHESSD
2, 7735–7772, 2014

Table 1. The inversion parameters with a set of used receivers (bold ciphers).

P	cond	r	err%	φ_{max}	φ_{min}	Receivers
3	100	41	71.7	1.213	−0.78	1,2,**3,**4,5,6,7,8,9,**10,**11,**12,**13,14
3	1000	42	74.8	1.577	−1.55	1,2,**3,**4,5,6,7,8,9,**10,**11,**12,**13,14
4	100	15	74.22	0.892	−0.655	1,2,**3,4**,5,6,7,8,9,10,11,**12,13**,14
4	1000	16	75.22	0.905	−0.647	1,2,**3,4**,5,6,7,8,9,10,11,**12,13**,14
4	100	34	99.1	0.128	−0.107	1,2,**3,4,5,**6,**7,**8,9,10,11,12,13,14
4	100	34	65.86	0.419	−0.156	1,**2,**3,4,5**6,**7,8,9,**10,**11,12,13,**14**
5	100	45	62.3	1.185	−0.67	1,2,**3,4**,5,**6,7**,8,9,10,**11**,12,13,14
5	1000	57	40.9	1.699	−0.75	1,2,**3,4**,5,**6,7**,8,9,10,**11**,12,13,14
5	1000	16	74	0.845	−0.69	1,2,**3,4**,5,**6,7**,8,**9**,10,11,12,13,14
9	100	73	37.7	1.539	−0.72	1,2,**3,4,5,6,7,8,9,10,11**,12,13,14
9	1000	104	63.3	2.396	−1.29	1,2,**3,4,5,6,7,8,9,10,11**,12,13,14
9	1000	104	59.9	2.25	−1.04	1,2,**3,4,5,**6,7,8,**9,10,11,12,13,14**
10	100	72	37.24	1.545	−0.645	1,2,**3,4,5,6,7,8,9,10,11,12**,13,14
10	1000	99	86.75	2.632	−1.909	1,2,**3,4,5,6,7,8,9,10,11,12**,13,14
10	1000	15	62.9	1.099	−0.74	**1,2,3,**4,**5,6,7,**8,**9,**10,11,**12,13,14**

The number of receivers is symbolized by P. Maximum and minimum values of the recovered function are symbolized by φ_{max} and φ_{min} respectively (scaled in m).

NHESSD
2, 7735–7772, 2014

Table 2. The inversion parameters with a set of seventh receivers (bold ciphers).

Model	cond	r	err%	φ_{max}	φ_{min}	Receivers
V1.1	100	23	62.8	1.106	−0.696	1,2,**3,4,5,6,7,8,9**,10,11,12,13,14
V1.2	10 000	32	51.9	1.392	−0.49	1,2,**3,4,5,6,7,8,9**,10,11,12,13,14
V2.1	100	73	37.7	1.559	−0.717	1,2,**3,4,5,6,**7,8,**9,10,11**,12,13,14
V2.2	10 000	92	32.7	1.686	−0.735	1,2,**3,4,5,6**,7,8,**9,10,11**,12,13,14
V3.1	100	65	45.9	1.449	−0.923	1,2,3,4,**5,6,7,8,9,10,11**,12,13,14
V3.2	10 000	104	26.7	1.816	−0.703	1,2,3,4,**5,6,7,8,9,10,11**,12,13,14
V4	10 000	59	31.73	1.706	−0.737	**1**,2,**3**,4,**5**,6,**7**, 8,**9**,10,**11**,12,**13**,14

The number of receivers is symbolized by P. Maximum and minimum values of the recovered function are symbolized by φ_{max} and φ_{min} respectively.

NHESSD
2, 7735–7772, 2014

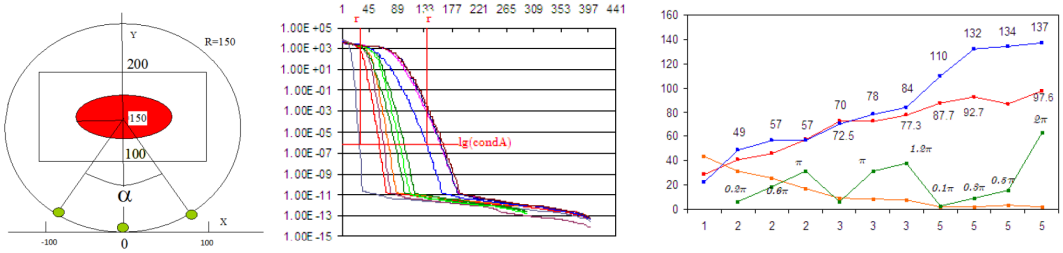

Figure 1. A layout scheme of the source-receivers arrangement (left). The common logarithm of the singular spectrum of the matrix **A** (vertical axis) in terms of the numbers of singular values (horizontal axis) and with different numbers of receivers used in the inversion: with one receiver (the dark blue line); with two receivers (the red, brown, orange lines); with three receivers (the herbal, light, dark green lines); with five receivers (the light blue, pink, dark blue, magenta lines) (middle). The inversion parameters in terms of the number of receivers: 100max of the recovered function (the red line), the values of number *r* (the blue line), misfit parameter (the orange line) and aperture angle (the green line) (right).

NHESSD
2, 7735–7772, 2014

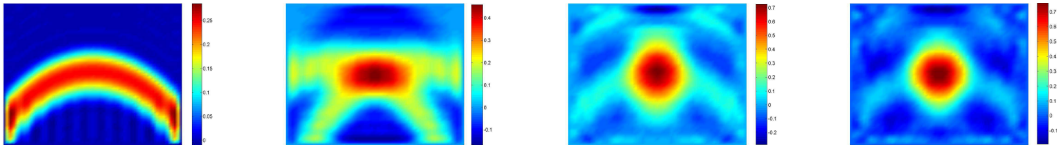

Figure 2. The recovered functions by the inversion: with one receiver (left); with two receivers, $\alpha = \pi/5$ (left middle); with three receivers, $\alpha = \pi/5$ (right middle); with five receivers $\alpha = \pi/10$ (right).

NHESSD
2, 7735–7772, 2014

Inversion method for initial tsunami waveform reconstruction

V. V. Voronin et al.

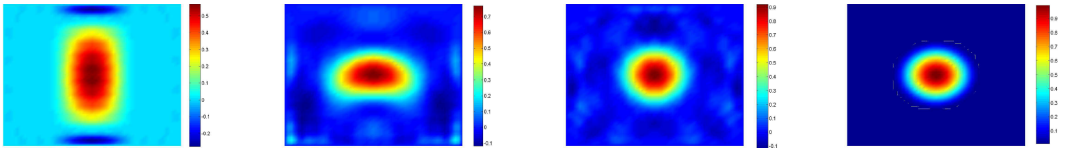

Figure 3. The recovered functions by inversion: with two receivers, $\alpha = \pi$ (left); with three receivers, $\alpha = \pi$ (left middle); with five receivers $\alpha = \pi/2$ (right middle); theoretical function (right).

NHESSD
2, 7735–7772, 2014

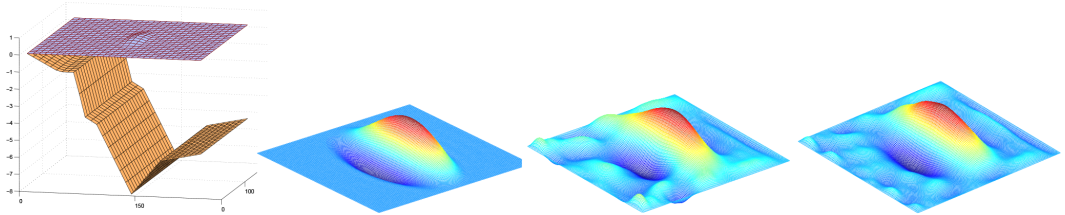

Figure 4. The model bottom topography having some basic morphological features typical of the island arc regions (left). The initial water displacement having the dipolar shape $\varphi_{max} = 0.73\,m$; $\varphi_{min} = 0.34\,m$; (middle left).The recovered function when three marigrams used: err% = 37.1 %; $\hat{\varphi}_{max} = 0.63\,m$; $\hat{\varphi}_{min} = -0.282\,m$; (middle right). The recovered function when five marigrams used: err% = 20.4 % ; $\hat{\varphi}_{max} = 0.71\,m$; $\hat{\varphi}_{min} = -0.289\,m$; (right).

NHESSD
2, 7735–7772, 2014

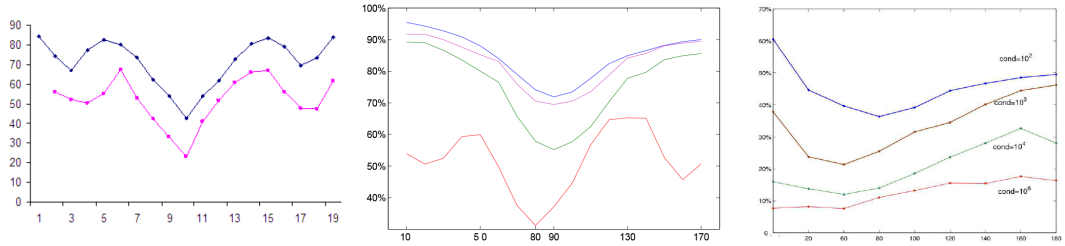

Figure 5. The misfit parameter err% in terms of the position of receivers on the aperture: with one receiver used (the blue line); with two receivers (the pink line); (left). The misfit parameter err% on a percentage basis for the case when two receivers were used in the inversion in terms of different rates of the background noise (p%) and the conditioning number of the matrix **A**: p = 0 %; cond(**A**) = 10^6 (the red line); p = 2.5 %; cond(**A**) = 1000 (the green line); p = 5 %; cond(**A**) = 1000 (the magenta line); p = 5 %; cond(**A**) = 100 (the blue line); (middle). The misfit parameter err% for Case (1) (three receivers) in terms of the conditioning number of the matrix **A** when p = 0 % (right).

NHESSD
2, 7735–7772, 2014

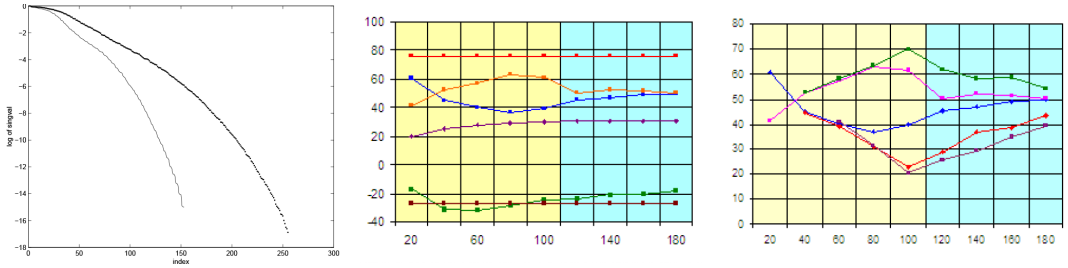

Figure 6. The singular spectra of the matrix **A** on the common logarithm scale when three (the thin line) and five (the thick line) receivers were used in the inversion (left). The inversion parameters when three marigrams used in terms of the aperture length (km): 100max (the top red line) and 100 min (the bottom red line) of the initial field; 100 min (the green line) and 100max (the orange line) of $\hat{\varphi}(x,y)$; err% (the blue line); number r (the dark blue line) (middle). The inversion parameters when five marigrams used in terms of the aperture length (km): err% (the orange line) and 100max (the green line) of the function $\hat{\varphi}(x,y)$ (case C3); err% (the violet line) (case C2); the inversion parameters when three marigrams used err% (the blue line) and 100max (the pink line) of the function $\hat{\varphi}(x,y)$ (right). The yellow color of columns are denote that aperture is placed inside the segment of the coast line corresponding to the projection of the source on the coast.

NHESSD
2, 7735–7772, 2014

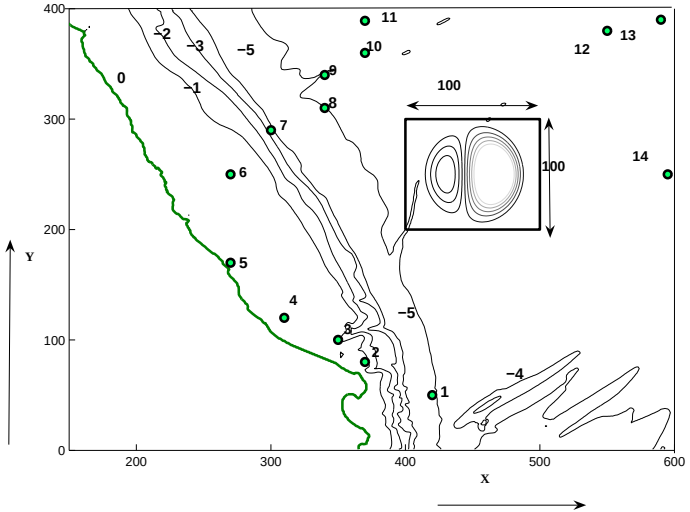

Figure 7. Isolines of the Peru subduction zone with depth values, the target domain and 14 receivers marked by the green color (∘); the green line indicates the coast line.

NHESSD
2, 7735–7772, 2014

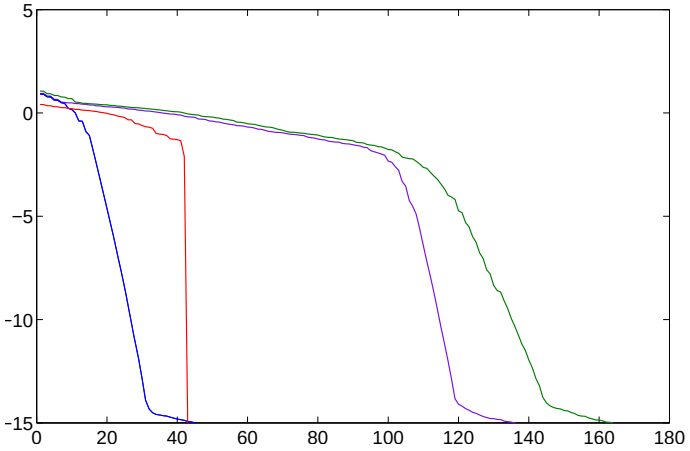

Figure 8. Typical graphs (upper parts) of singular values in the common logarithm scale of the matrix **A** with respect to their numbers when the number of marigrams used in the inversion is equal to: three (the red line); four (the blue line); nine (the violet line) and ten (the green line).

NHESSD
2, 7735–7772, 2014

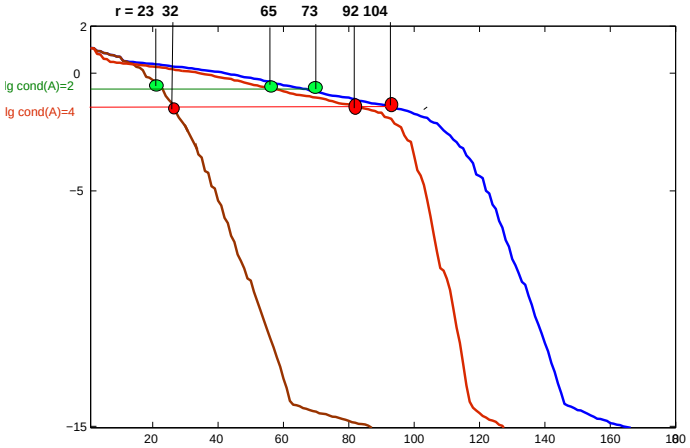

Figure 9. Singular spectra in the common logarithm scale for the models: V1.1 and V1.2 (the brown line), V2.1 and V2.2 (the red line); V3.1 and V3.2 (the blue line); the red color and the green color (∘) point to the value r selected for cond(**A**) = 10 000 and for cond(**A**) = 100, respectively.

NHESSD
2, 7735–7772, 2014

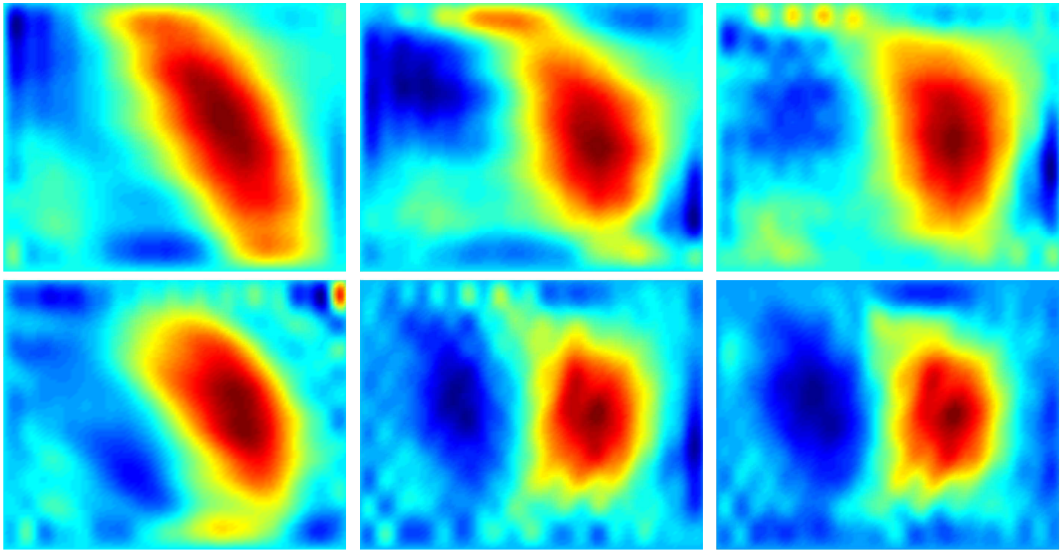

Figure 10. The recovered functions: cond(**A**) = 100 (top) by models V1.1 (left), V2.1 (middle) and V3.1 (right); cond(**A**) = 10 000 (bottom) by models V1.2 (left), V2.2 (middle) and V3.2 (right).

NHESSD
2, 7735–7772, 2014

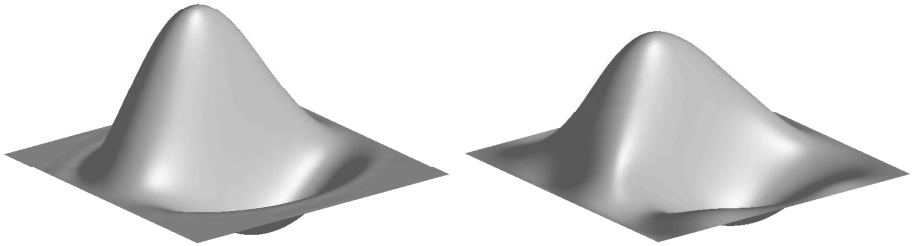

Figure 11. Theoretical tsunami source model: $\varphi_{max} = 1.959\,m$; $\varphi_{min} = -0.67\,m$; (left). Model V3.2 $\hat{\varphi}_{max} = 1.816\,(1.514)\,m$; $\hat{\varphi}_{min} = -0.707\ (-0.548)\,m$; $r = 104$; $\mathrm{cond}(A) = 10^4$; (right). The values in parentheses are extreme values of the recovered waveform after smoothing.

NHESSD
2, 7735–7772, 2014